Prepared for the National Institutes of Health
National Institute of Neurological Disorders and Stroke
Division of Fundamental Neurosciences
Neural Prosthesis Program
Bethesda, MD 20892

Unassisted Standing with Functional Neuromuscular Stimulation

NIH-NINDS-N01-NS-6-2351

Progress Report #4

Period Covered:
October 1, 1997 – December 31, 1997

Principal Investigator: Ronald J. Triolo, Ph.D.[1]
Co-Principal Investigators: Robert F. Kirsch, Ph.D.[2]
John A. Davis, Jr., M.D.[1]

Departments of Orthopaedics[1] and Biomedical Engineering[2]
Case Western Reserve University
Cleveland, OH 44106-4912

Co-Investigators: James J. Abbas, Ph.D.
University of Kentucky

Scott L. Delp, Ph.D.
Northwestern University

I. ABSTRACT

The long-term goal of this contract is to develop methods to provide brace-free, energy efficient standing for persons with complete thoracic level spinal cord injuries via functional neuromuscular stimulation (FNS). The resulting system will resist reasonable disturbances and maintain balance automatically while allowing free use of the upper extremities to manipulate objects in the environment. These objectives are being addressed through an organized effort consisting of anatomical and dynamic modeling, control simulation and optimization, and experimental demonstration of new control structures. The work represents an active partnership between investigators at Case Western Reserve University (CWRU) and collaborators at Northwestern University and the University of Kentucky.

II. INTRODUCTION

Achieving independent, hands-free standing with FNS depends upon the development of an anatomical and dynamic model of the lower extremities and torso. This model will be employed to construct dynamic simulations and perform optimization procedures to investigate the theoretical behavior of various FNS control systems for providing automatic postural adjustments. Goals for the second year of the contract include: a) refining the anatomical model of the trunk and integrating it into the representation of the lower extremities using Software for Interactive Musculoskeletal Modeling (SIMM Musculographics Inc.), b) validating the resulting dynamic model and simulating the actions of various automatic postural control systems, c) optimizing controller performance, incorporating the actions of FNS and the effects of spinal cord injury (SCI), and d) characterizing baseline performance of open-loop and feed-forward standing systems.

Substantial progress has been made in modeling the musculoskeletal anatomy of the trunk, preparing experimental procedures for validating the three-dimensional dynamic standing model, determining the input-output characteristics of body-mounted sensors for simulation and control, and extending the model to account for passive joint properties which may be significant in the SCI population. In large part, efforts have concentrated on readying the software and experimental methods required to initiate human testing with able-bodied volunteers and individuals with SCI who are standing with simple continuous stimulation systems. This report summarizes these results and their relationship to the overall goals of the contract.

III. PROGRESS THIS REPORTING PERIOD

Progress this reporting period was made primarily in three areas: 1) anatomical modeling of the torso, 2) dynamic biomechanical modeling and simulation for control, 3) sensor evaluation and characterization.

A. Anatomical Modeling of the Torso

We previously reported the results of our initial effort to develop models of the trunk muscles from specimens gathered from a fresh-frozen cadaver at MetroHealth Medical Center.

Detailed analyses of the erector spinae, quadratus lumborum and rectus abdominus muscles have since been completed. The morphometric parameters that determine the force-generating capacity of a muscle (such as physiologic cross-sectional area, pennation angle, and optimal fiber length) were measured for the specimens harvested during the dissection. The model of the erector spinae was significantly revised based on this in-depth anatomical study. The SIMM model of the trunk was updated with the revised descriptions of the muscle geometry and the newly measured muscle parameters.

1. Revisions of muscle geometry: During the dissection, three major columns of the erector spinae in the thoraco-lumbar region were identified (spinalis thoracis, longissimus thoracis, and illiocostalis lumborum). The previous SIMM model of the erector spinae consisted of three columns: spinalis thoracis, illiocostalis thoracis, and illiocostalis lumborum. The dissection clearly showed that the longissimus thoracis would be a major contributor to *both* thoracic and lumbar motion, whereas the illiocostalis thoracis would contribute to motion *only* at the thoracic levels. Therefore, the SIMM model of the erector spinae was modified to include the longissimus thoracis instead of illiocostalis thoracis.

2. Measurement of muscle parameters: The parameters we measured from each muscle were musculotendon length, muscle length, pennation angle, and fascicle length. The musculotendon length was measured as the distance between the most proximal tendon and the most distal tendon. The muscle length was the length between the most proximal fiber to the most distal fiber. The pennation angle was defined as the angle made by the fibers with the muscle line of action. Ten fibers were studied for each muscle and the average of their lengths was defined as average fiber length. The muscle sarcomere length was determined using a laser diffraction method. A 5mW He-Ne laser was shown through a slide containing a small piece of each fascicle. The width of the first order diffraction pattern was recorded. The sarcomere length was calculated as:

$$Ls = \lambda / \sin\theta$$

where Ls is the sarcomere length, λ is the wavelength of the laser (0.632 μm) and θ was calculated using:

$$\theta = \tan^{-1} (y / L)$$

where y is the width of the diffraction pattern and L is the distance (7.56 cm) between the slide and the glass where the pattern is formed. Twelve sarcomere measurements were obtained for each of the ten fibers (120 measurements for each muscle). The 120 measurements were averaged to obtain the average sarcomere length for the muscle. The optimal fiber length was calculated as the average fiber length multiplied by the ratio of the optimal sarcomere length for mammalian muscle (2.8 μm) and the average sarcomere length calculated for the particular muscle. The weight of the muscle without the tendon (muscle fiber only) was measured to calculate the physiologic cross-section area (PCSA). PCSA was defined as:

$$PCSA = mass / \rho * l_{om}$$

where ρ is the density of muscle tissue (1.06 g/cm^3) and l_{om} is the optimal fiber length.

Results of the analysis and measurement of architectural and morphometric parameters for the erector spinae and other muscles of the torso and abdomen are summarized in **Table 1**. The erector spinae aponeurosis gives rise to the longissimus thoracis and the illiocostalis lumborum. The two columns emerge as individual muscle units around the T10-T11 region. The deep surface of the muscle reveals the fibers of the two columns branching into different directions. The longissimus thoracis had a musculotendon length of 37.6 cm and a muscle length of 31.1 cm. The pennation angle measured from the superficial surface was 22°. On the deep surface fibers were pennated in the range of 0° (more proximal) to 25° (more distal). The average fiber length was measured as 10.0 cm and the average sarcomere length was 2.5 μm. The PCSA was calculated to be 3.79 cm^2 and the optimal fiber length was 11.2 cm. The musculotendon length of illiocostalis lumborum was 37.6 cm and the muscle length was 28.5 cm. The pennation angle was 10°, but ranged from 0-15°. The average fiber length was 11.9 cm and the average sarcomere length was 2.47 μm. The PCSA was calculated as 3.39 cm^2 and the optimal fiber length was 13.5 cm.

Table 1. Muscle Architecture for Selected Muscles of the Torso and Abdomen

	Spinalis Thoracis	Longissimus Thoracis	Illiocostalis Lumborum	Rectus Abdominus	Quadratus Lumborum (proximal)	Quadratus Lumborum (distal)
Musculotendon Length (cm)	25.0	37.6	37.6	34.3	10.9	8.5
Muscle Length (cm)	14.0	31.1	28.5	33.0	10.5	8.4
Pennation Angle (degrees)	18	22	10	0	0	0
Mean Fiber Length (cm)	5.2	10.0	11.9	27.9	6.2	4.2
Mean Sarcomere Length (μm)	2.5	2.5	2.5	3.6	2.9	2.9
PCSA (cm^2)	0.88	3.79	3.39	1.95	1.09	0.93

Musculotendon Length: Distance between most proximal and most distal tendon
Muscle Length: Distance between the most proximal and the most distal muscle fiber
Pennation Angle: Angle between the fibers and the muscle line of action
Mean Fiber Length: Average of 10 fibers from each muscle
Mean Sarcomere Length: Average of 120 sarcomere measurements using laser diffraction
Physiologic Cross Sectional Area: muscle volume/optimal fiber length.

The rectus abdominus was observed to have two tendinous infractions. It was difficult to trace a single fiber from the origin to insertion because of the infractions; therefore, the muscle was divided into portions (proximal, middle, and distal) based on these infractions. On the medial edge, the proximal infraction was 5.8 cm from the proximal end of the muscle. The distal infraction was 10.5 cm from the proximal end of the muscle. Ten fibers were removed from each portion. Six sarcomere measurements were made from each fiber. The PCSA of the total muscle was calculated as the average of the three portions.

Table 2 summarizes the muscle parameters measured from the rectus abdominus. The musculotendon length of the overall rectus abdominus was 34.3 cm. The muscle length was observed to be 33.0 cm. The fibers were arranged uniformly along the muscle line of action, therefore the pennation angle for all segments was 0°. The fiber lengths, sarcomere lengths, optimal fiber lengths and PCSAs varied from segment to segment, as shown in **Table 2**. Average fiber and sarcomere lengths for the whole muscle were 27.9 cm and 3.6 cm, respectively. The average PCSA of the entire rectus abdominus was 1.95cm^2 and the optimal fiber length at neutral position was 19.4 cm.

Table 2. Measurements of Muscle Architecture for Rectus Abdominus

	Proximal Segment	Middle Segment	Distal Segment	Average for the Muscle
Musculotendon Length (cm)	-	-	-	34.3
Muscle Length (cm)	-	-	-	33.0
Pennation Angle (degrees)	0	0	0	0
Mean Fiber Length (cm)	5.5	4.6	17.8	27.9
Mean Sarcomere Length (μm)	3.5	3.7	3.6	3.6
PCSA (cm^2)	2.36	2.28	1.73	1.95

3. Summary and immediate plans: The muscle parameters have been defined based on the analyses performed on a single cadaver. Efforts are underway to compare the forces generated by the muscles as predicted by the current model to published data. Dissection and similar detailed analyses will be performed on a second specimen in March 1998. Collection of data from three to 5 cadavers of various sizes will help us better understand the variation of muscle architectural parameters from one subject to another. After completing the anatomical modeling, the torso model will be combined with the existing lower extremity model as an integrated tool for whole-body dynamic simulation. This will be followed by experimental evaluation and further refinement of the trunk model.

B. Biomechanical Modeling and Simulation

In previous reports we described the development of a dynamic, three-dimensional, closed-chain model of the two human lower extremities and demonstrated the feasibility of using it to perform control simulations. This resulted in the successful construction of a joint angle based PID controller capable of simulating the transfer from one posture to another and maintaining upright balance. Techniques were developed to estimate the postural disturbances caused by volitional upper extremity movements, and initial plans to evaluate the model were described. The current reporting period has been dedicated in large part to preparing the procedures and laboratory hardware and software required to evaluate these elements of the

model experimentally. In addition, work on the joint angle based PID controller has been extended through a simulation study of the relative moment generating capacities of individual muscles around each joint. Such quantitative information will be critical to determining efficient patterns of muscle activation and minimizing energy consumption, while assisting with the selection of the most effective targets for stimulation. Finally, procedures have been developed for the experimental measurement the passive properties of the joints, which are currently not included in the biomechanical model and may be significant to individuals with spinal cord injuries.

1. Data acquisition system for experimental testing of the 3-D dynamic standing model: Our approach to testing, as previously described, includes using electromyographic activity measured during standing maneuvers as activation levels in a forward simulation that will result in estimates of joint moments. Kinematic and kinetic data measured simultaneously will be used to estimate joint moments through inverse dynamics. The results of both analyses will be compared to assess the accuracy of the biomechanical model. An integrated data acquisition system was developed in preparation for this experimental evaluation of the lower extremity model. The laboratory hardware consists of three subsystems responsible for measuring kinematics, ground reaction forces and moments, and electromyographic (EMG) activities, respectively, along with the software to coordinate their actions. The system is depicted schematically in **Figure 1**.

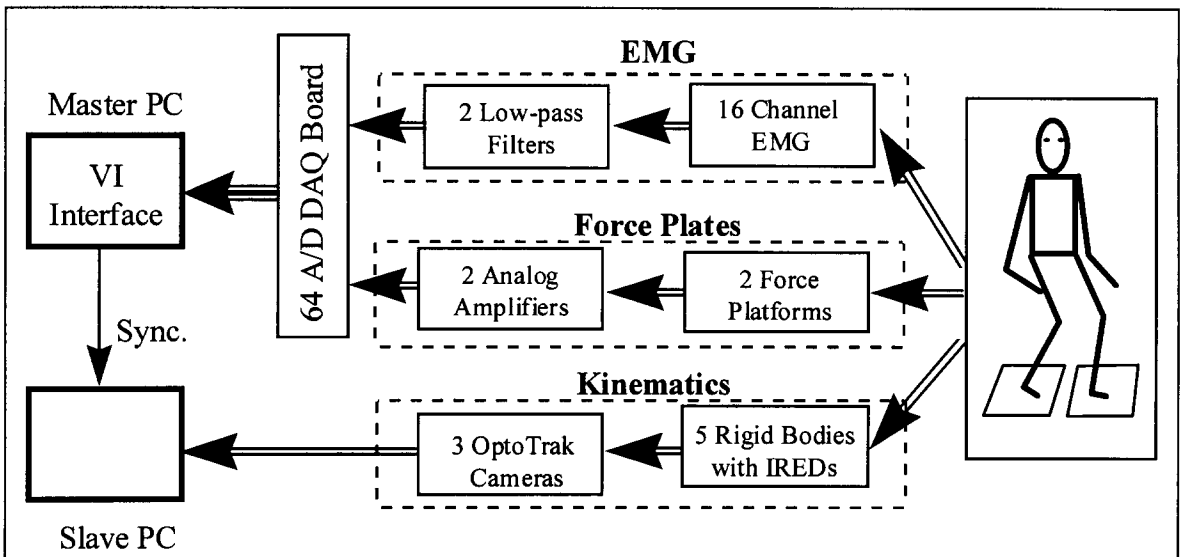

Figure 1: Integrated Data Acquisition System for Bipedal Model Evaluation

The purpose of the kinematic measurements is to obtain time histories of joint angles, angular velocities, and angular accelerations. In our experimental design, these angular variables will be calculated from estimates of individual limb segment positions provided by an OptoTrak motion analysis system (Northern Digital, Inc.) using rigid body concepts. The OptoTrack detects the positions of infrared light emitting diodes (IREDs) affixed to rigid bodies that are attached to the limbs. We have fabricated five rigid bodies using thermoplastic material (Johnson & Johnson, Inc.) that will be attached to the shanks, thighs, and right upper arms of able bodied test subjects. Four IREDs are mounted on each rigid body to insure that at least three

of them are visible to the OptoTrak cameras at all times during data collection. The OptoTrak system is operated at a sampling frequency of 100Hz.

The ground reaction forces and moments are measured by two biomechanics platforms (AMTI, Inc.). Two force plates are required to validate the model in three dimensions. Knowledge of ground reaction forces and moments at both feet will allow us to conduct inverse dynamics calculations for each leg separately, rather than assuming that they move symmetrically and calculating forces and moments averaged over both legs. This will permit us to evaluate the performance of the technical innovations employed in the model to satisfy the constraints imposed by a closed kinematic chain. Another advantage of using two force plates is that the calculated joint reaction forces and moments at both hip joints can be used to check the estimated body inertial properties of the trunk. The force plates are operated at sampling frequencies in multiples of 100Hz to facilitate synchronization of the kinetic data with the kinematics obtained from the OptoTrack.

If a force plate is not mounted horizontally, its normal reaction force will not be vertical and errors will be introduced into the experimental measurements. For this reason, the position and orientation of the biomechanics platforms were measured in the laboratory with the OptoTrak system. Four IREDs were mounted on the surface of each platform. The resulting measured coordinates in the frontal and sagittal planes are plotted in **Figure 2**. The maximum vertical difference between IREDs is less than 1.39 mm, which occurred between markers that were more than 700 mm away from each other. This represents an angle of approximately 0.1 degree and indicates that the instruments are sufficiently level for experimental work to proceed.

Figure 2: Position and Orientation Calibration for the Biomechanics Platforms

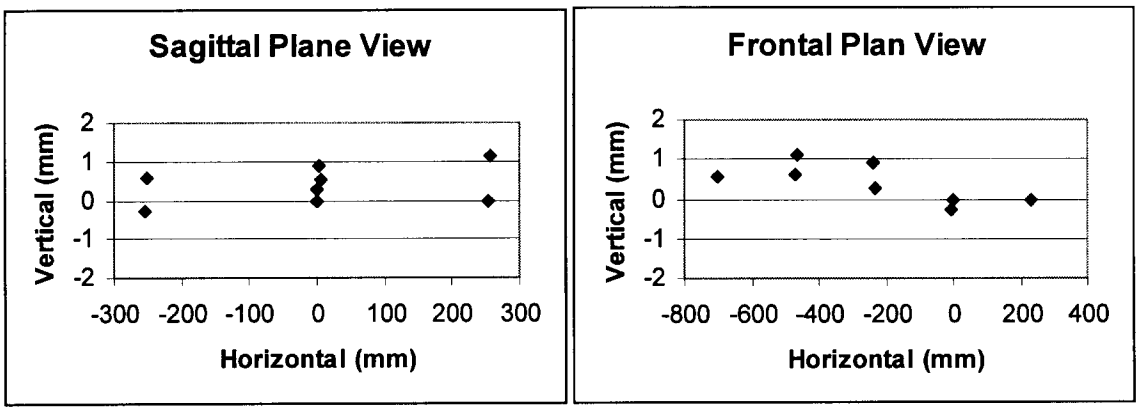

EMG signals will be collected to provide qualitative and quantitative information regarding muscle activation levels in the dynamic simulations. Eight major muscles on each leg, including soleus, gastrocnemius, tibialis anterior, vasti, semimembranousis, posterior portion of the adductor magnus, gluteus maximus, and gluteus medius, have been selected based on their accessibility by surface EMG electrodes. We have designed and fabricated EMG preamplifiers for these experiments, as well as the appropriate isolation and amplification stages for 16 channels of data. Two 8-channel programmable analog filters (IOtech, Inc.) with Bessel-response characteristics have been recently purchased and integrated into the laboratory instrumentation for EMG signal conditioning.

As **Figure 1** shows, the data acquisition system requires the coordination of two separate personal computers. The first (master) PC uses a 64 channel data acquisition board (National Instruments Corporation) to collect analog signals from the surface EMG and biomechanics platforms simultaneously. A virtual instrument interface was designed in LABVIEW to collect and display the signals. In order to reduce noise and increase common-mode noise rejection, a differential configuration was chosen for the input channels. The second (slave) PC operates the OptoTrak system and runs dedicated data collection software in parallel to the master PC. Synchronization between the computers is achieved by sending a digital trigger signal from the master to the slave.

All three subsystems and the virtual instrument interface have been tested experimentally. Throughout the remainder of the contract year, the focus of this effort will shift to evaluating the model with real data. Simulation and optimization studies will be performed in parallel to the experimental testing.

*2. **Relative moment generating capacity of postural muscles**:* During the current period, we have further developed the joint angle based PID controller for transferring posture and maintaining balance. As a first attempt to minimize energy consumption and extend elapsed standing time, we are modifying the design of the controller weight matrix to reflect the relative strengths of prime movers at each joint to increase efficiency. In this control system, the outputs from individual PID controllers were further multiplied by the controller weight matrix to regulate activation and distribute the required joint moments among individual muscles (see details in Figure 4, Report #3). In the preliminary design, individual muscles were treated equally so that each muscle has equal weight in terms of its contribution to total joint moment. This was not optimal since muscles have different strengths and joint moment generating capacities. To refine the design, we have analyzed the relative strength of each muscle within the range of joint angles around the standing position using the able-bodied muscle mechanics model in SIMM.

The major muscle groups affecting six joint angles (two at ankle, one at knee, and three at hip) were identified and the isometric joint moments for each muscle were simulated at a full activation over the ranges of motion representing small variations around the upright position. **Figure 3** summarizes the relative ankle, knee and hip moments of the major contributors at each joint. We are using this quantitative information to refine the control weighting matrix and perform several theoretical optimization studies.

*3. **Adapting the model for SCI and FNS – measuring passive joint properties:*** The contribution of passive moments to the total joint moments needed during standing and the transitions between standing and sitting have long been assumed to be negligible [1-3, 5]. This is still an open question for able-bodied individuals, and will only be compounded in persons with spinal cord injuries for two reasons: a) Passive properties are likely to be exaggerated by the extended immobility resulting from paralysis and b) Even after extensive exercise, the maximal muscle forces produced with FNS will be a fraction (typically 50% or less) of nominal maximal voluntary contractions. Consequently, the passive moments may become more of a significant factor in the total joint moment required for standing. The current form of the bipedal biomechanical model does not include the passive joint properties. Quantifying the influence of

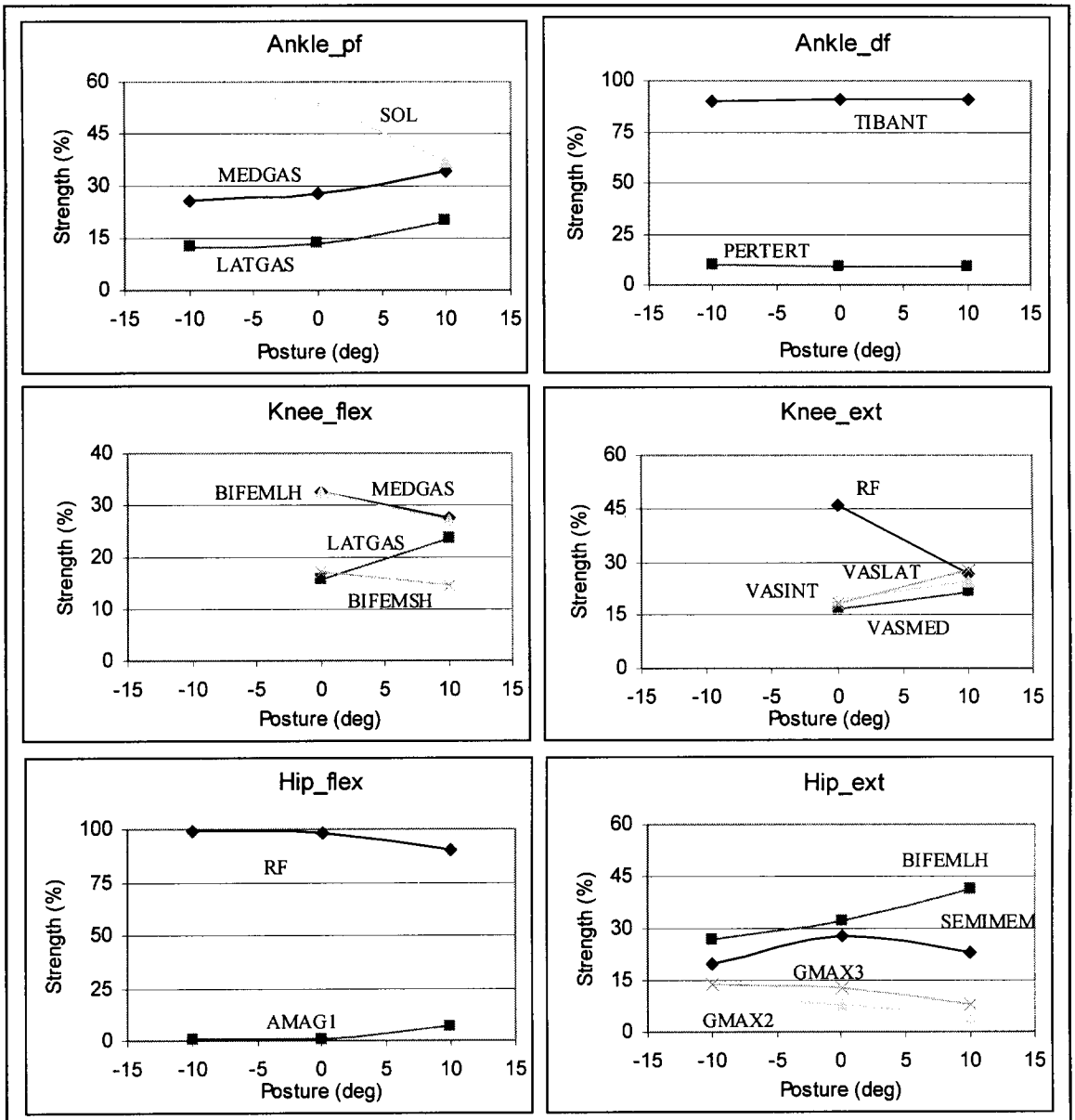

Figure 3: Relative Isometric Moment-Generating Capacities of Postural Muscles

these properties is critical for developing a realistic model, especially one suited for simulating standing with FNS in individuals with SCI.

We have begun to address the question of the significance of passive moments in the lower extremities by identifying the instrumentation and methods to measure them. The KinCom® (Chattex, Inc.) robotic dynamometer in the General Clinical Research Center at MetroHealth Medical Center is capable of a) imposing various fixed angular velocities upon a joint over the range observed during standing, b) positioning the ankle, knee or hip joints at various angles, and c) providing adequate force resolution for our purposes. The KinCom® was tested to determine its ability to perform the required isokinetic and stress-relaxation tests to determine the passive properties of the joints of interest. Various experimental set-ups were

simulated successfully with the device, which will be used extensively in the future to measure the passive moments in able-bodied volunteers as well as individuals with spinal cord injuries.

To prevent our measurements from being corrupted by voluntary or involuntary muscle activity, surface EMG of the relevant muscle groups will be monitored during the experimental sessions. Because the KinCom® data acquisition system has only two dedicated EMG channels, we will sample position, velocity and moment signals along with various EMG signals with our own data acquisition system in parallel to the operating system of the dynamometer. To this end, we have designed the appropriate isolation amplifier and buffer circuitry to protect the subject and to insure the integrity of the signals acquired by our system.

The experimental protocols to measure the passive moments at the hip, knee and ankle were also finalized during this period. The joint velocity, joint angle, angle of approach, and adjacent joint angle(s) will be varied to determine how these parameters affect the passive moments. Varying these parameters will also enable us to separate out the contributions of the elastic, plastic, and viscous components. A set of pilot tests was performed to obtain preliminary data regarding the passive properties of the ankle joint while finalizing the protocol and verifying the capabilities of the KinCom®. Data from one of the pilot tests is presented in **Figure 4**. Although the angular excursion was smaller than the subject's full range of motion, a clear dependence on the joint position was still observed. The passive moment increased rapidly as the joint rotated to the end of its dorsiflexion range. A similar result would also have been seen

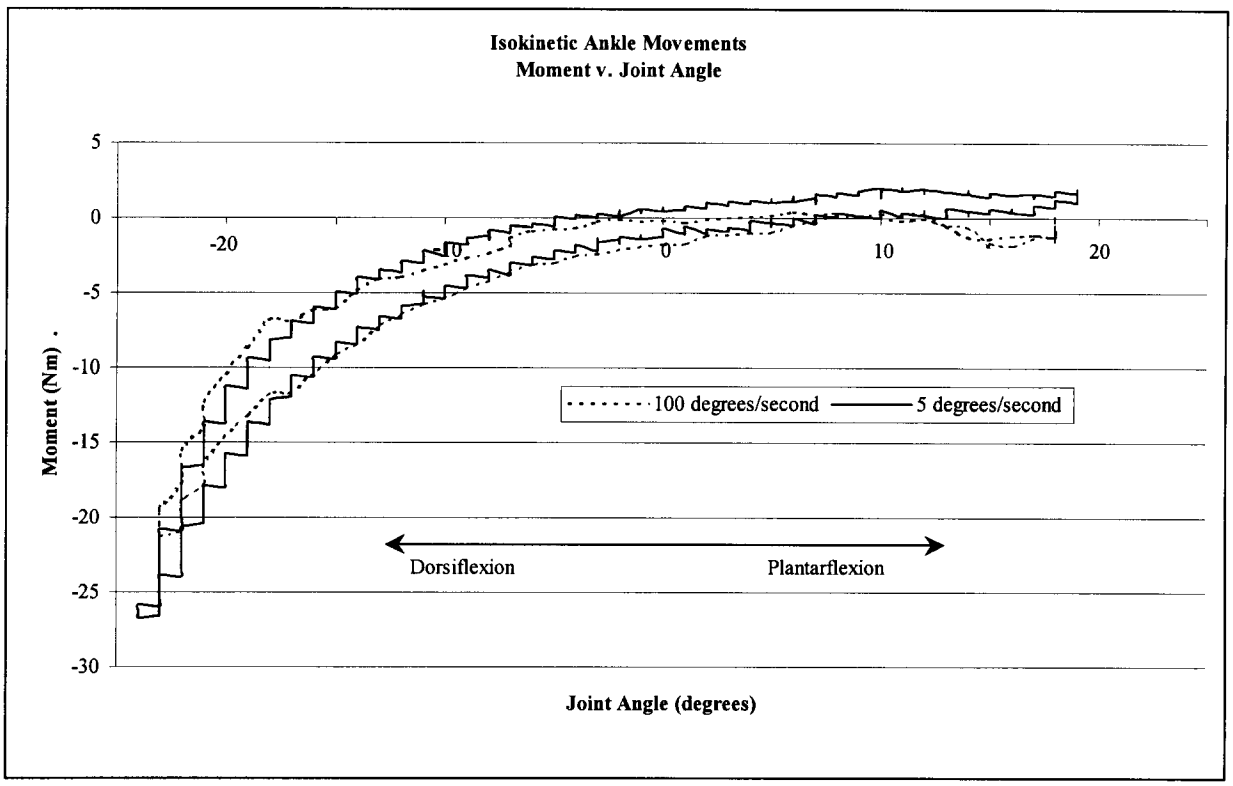

Figure 4: The effect of joint velocity on passive moments measured at the ankle. The data suggest that the angular velocity of the joint has a negligible effect on the passive moment. Further testing will quantify its influence.

in the plantarflexion direction if the ankle had been rotated through its full range of motion. The dependence of passive moment on joint velocity is also evident in **Figure 4**, which depicts the moments measured at two speeds (5 °/s and 100 °/s). The differences due to the velocity appear to be small, agreeing with reports stating that velocity effects are negligible [5,7]. Elements of **Figure 4** coincide with other data found in the literature in several other respects, thus validating our experimental design. The range of data from the 5°/s graph with the ankle at 12° and the knee at 90°overlaps with that reported in [4] and is within one Nm of the static values reported in [6] with the ankle fixed at 12°.

We plan to begin measuring the passive moments in able-bodied volunteers in the near future. This will be followed by repeating the same experiments on a sample of volunteers with spinal cord injuries. Using the collected data, empirical equations will be developed to describe the passive moments generated at each joint and their dependence on the previously mentioned variables (e.g. joint angle and joint velocity). These equations will be incorporated into the overall biomechanical model and the significance of the passive contributions will be examined in simulation. We will then proceed to examine the active contractile properties of stimulated paralyzed muscle in an effort to continue refinement of the model.

C. Sensor Characterization

Several of the control strategies to be investigated in this project will utilize sensors attached in some manner to the body. We have obtained several different sensors and have devised experimental protocols for characterizing the input-output properties of these sensors in isolation and when attached to the body. These input-output properties will then be incorporated into computer simulations with our model of the lower extremities and trunk, and the impact of the various sensor properties on unassisted standing by FNS will be quantified for different controller algorithms. These results will allow us to determine whether sensor properties and/or body attachment issues limit overall controller performance, and perhaps will suggest needed improvements in sensor properties. Progress in this area has included 1) obtaining body mounted sensors or establishing relationships with sensor developers, 2) specification of procedures for characterizing the devices, and 3) completing the evaluation of a commercially available gyroscope.

1. Procurement of device and establishment of relationships with sensor developers: We have obtained an integrated three-dimensional accelerometer unit from Analog Devices, Inc. (Norwood, MA), a prototype three-dimensional orientation sensor from Microstrain, Inc. (Burlington, VT), and a foot force sensor from Cleveland Medical Devices, Inc (Cleveland, OH). The Analog Devices and Microstrain devices are small enough to be conveniently mounted onto the lower extremities and/or trunk, while the Cleveland Medical Devices insert is incorporated into an insole that can be simply placed within the shoe. All of these devices have the desirable property of avoiding the spanning of joints.

The Analog Devices 3D accelerometer unit (ADXL05EM-3) is small and simple to use because the excitation and amplification electronics are integrated into the unit. The user provides only a single supply voltage, and the unit outputs the three orthogonal accelerations. This device will be used primarily to measure the acceleration of the torso for implementation of a feedforward controller to minimize the effects of unexpected disturbances, but it could also be

used to estimate joint angles (relative to earth's gravity field) during posture and slow movements if separate units are attached to adjacent limb segments.

The Microstrain orientation sensor (3DM) is not yet commercially available and we have agreed to evaluate pre-production prototypes for use in biomechanics applications. The novel devices uses three-dimensional measurements of earth's gravity and magnetic fields to compute absolute orientation in terms of roll, pitch, and yaw angles. They also include an integrated serial interface that allows several of them to be conveniently networked together. Placing these devices on adjacent body segments will allow measurement of joint angles (i.e., relative changes in orientation of adjacent body segments) rather than just absolute body segment orientations. Because this device also provides 3D acceleration signals, it could be mounted to the torso to estimate its acceleration as well as its orientation. We currently have received one such device, but will receive a total of 8 devices during the first quarter of 1998.

The Cleveland Medical Devices sensor consists of a thin flexible insole instrumented with deposits of pressure-sensitive resistive ink. The resistive elements sense the forces applied between the foot and the shoe (or floor) directly under the major weight-bearing points of the foot: the 1st metatarsal head, 5th metatarsal head, and the lateral and medial portions of the heel. Previous work has indicated that the 8 signals provided by two devices (one under each foot) will provide accurate estimates of the center of pressure (COP) of the body. We have therefore obtained 2 of these devices for testing.

We have also investigated the use of optical gyroscopes to measure joint velocities and angles. These devices have the advantage of being insensitive to inertially-related inputs. However, because they are primarily velocity sensors position (e.g., joint angle) estimates must be obtained by numerical integration, a process that is prone to offsets and drift. A collaboration with Rice Systems, Inc. for the development of an optical gyroscope suitable for closed-loop control of lower extremity and trunk FNS has been initiated. This project is outside the scope of this contract, although its outcome is obviously relevant.

2. Definition of characterization procedures for body mounted sensors: We will characterize each of the above-mentioned sensors both in bench tests and during real tasks when attached to the body. The bench tests will characterize the basic transducer properties of the sensor and lead to a mathematical model of the sensor in isolation. The performance of the sensors when mounted on the body will determine the effects of 1) misalignment between the sensitive axes of the sensor mounted on a limb segment with the actual movement (e.g., joint angles or body accelerations) being measured and 2) relative motion between the sensor and the underlying bones because of the compliant properties of skin, subcutaneous fat, and muscle.

Detailed protocols and test results for each device will be described in future reports. Briefly, bench tests will use controlled inputs (positions, orientations, accelerations, forces, etc.) and independent measurements of each relevant sensor output under highly constrained conditions to obtain input-output properties for each sensor signal. Each sensor will then be represented by a mathematical model that includes any nonlinearities, inherent noise, dynamic properties (of the device and any needed signal processing such as filtering), and off-axis sensitivities. Motion sensor performance when mounted to the body will be compared to measurements obtained using the OptoTrak motion analysis system. Redundant OptoTrak markers can be mounted to minimize both alignment errors and the impact of soft-tissue movement, and thus will serve as a reasonable standard against which to compare the body

mounted sensors. The performance of the foot-force sensor in estimating center of pressure will be compared to that obtained from a pair of commercial force plate sensors (AMTI, Inc.). For both the motion and center of pressure sensors, the properties of the interface between the sensor and the underlying bony elements will be characterized by the relationship between the standard measurement (i.e., OptoTrak or force plate) and the corresponding sensor signal. This relationship will include coordinate transformations (i.e., misalignment) and dynamic properties (phase shifts and/or delays due to soft tissue movement). For all sensors, several relevant conditions will be examined, including quiet standing, sit-to-stand and stand-to-sit transitions, and voluntary swaying, crouching, and leaning movements.

Once the sensor characterizations are complete, the resulting models of the sensors themselves and of the interface between the sensors and the underlying skeletal members will be incorporated into the overall computer simulations which also include the lower extremity and trunk body model and various FNS controllers. In addition to judging the likely effectiveness of each controller itself, sensitivity analyses will be performed to determine whether sensor properties or sensor-skeletal interface properties are limiting overall performance. If not, this indicates that existing sensors will likely be adequate for our applications. If so, modifications can be made in the modeled sensor until overall performance is acceptable, and the suggested improvements in either the sensor itself or in its attachment to the body can be pursued.

3. Evaluation of a commercially available gyroscope for obtaining kinematic measurements: In this quarter, we have begun to evaluate an inexpensive, commercially available gyroscope that consists of two single-axis gyroscopes mounted on a single board. This unit is currently utilized in the Gyropoint mouse [Gyration, Inc.] and the gyroscopic sensors themselves are produced by Murata Corp., but are not available from the manufacturer in small quantities. We extracted the board from the mouse (approximate board dimensions 4.5 cm x 2 cm x 1 cm) and have made appropriate connections for power supply and recording of output channels. The unit generates a voltage signal (0-5V) that provides a measure of angular velocity of the sensor.

For the evaluation, the sensor was mounted in a small plastic box (dimensions: 10cm x 5cm x 2.5cm) which was attached to the arm of a plexiglass calibration device. With this device, the arm can be placed at specific known angular orientations (10° increments from -80° to 100° with 0° defined as vertical) or the arm can be rotated about a pivot while recording from a potentiometer mounted at the joint. Thus, we can obtain a set of static measurements at known angles and then continuously collect data from the gyroscope and the potentiometer to evaluate the dynamic response of the sensor.

The voltage signals from both the gyroscope and the potentiometer were collected at 100 samples/sec under a variety of conditions. The voltage signals recorded in one trial are presented in **Figure 5**. After subtracting the offset voltage from the gyroscope, the recorded voltage signal was then integrated. A linear regression (integrated voltage and static angle measurements) was used to calculate the slope of a linear calibration curve. Results indicate a very good linear fit (R^2=0.99) over the range of 180°. A similar calibration (without the integration) was performed for the potentiometer signal.

In subsequent trials, the following equation was used to determine angle measurements from the gyroscope voltage readings:

$$\theta_g(t) = m_g(\int(v_g(t) - v_o)) + \theta_o$$

Where $\theta_g(t)$ is the angle estimate from the gyroscope, $v_g(t)$ is the voltage reading from the gyroscope, v_o is the initial voltage (assumes zero velocity), m_g is the gain calculated from the static calibration, and θ_o is the initial angle (which is assumed to be known).

Figure 6 depicts the angle estimates from both the gyroscope and potentiometer during angular rotations over a range of approximately 100°. The RMS value of the difference between the two signals over the first 10 seconds of the trial was 1.4°; while the RMS error over the last 10 seconds of the trial was 9.6°. These data are consistent with other data that we have collected and indicate that the gyroscope can give very good estimates of joint angle for short periods of time, but that on occasion, a drift in output is observed. We are currently investigating the source of the drift and techniques to remove it or to account for it.

In conclusion, these sensors may be suitable for use in detecting angular orientation of limb segments during stance. Results indicate that there are intermittent problems with drift in the angle estimates. We are currently investigating methods of addressing this issue. Over the next several months, we plan to continue the evaluation of gyroscope, complete the setup of the laboratory hardware and software required for the experimental characterization of the open-loop control system using the posture-shifting paradigm and to begin these experiments.

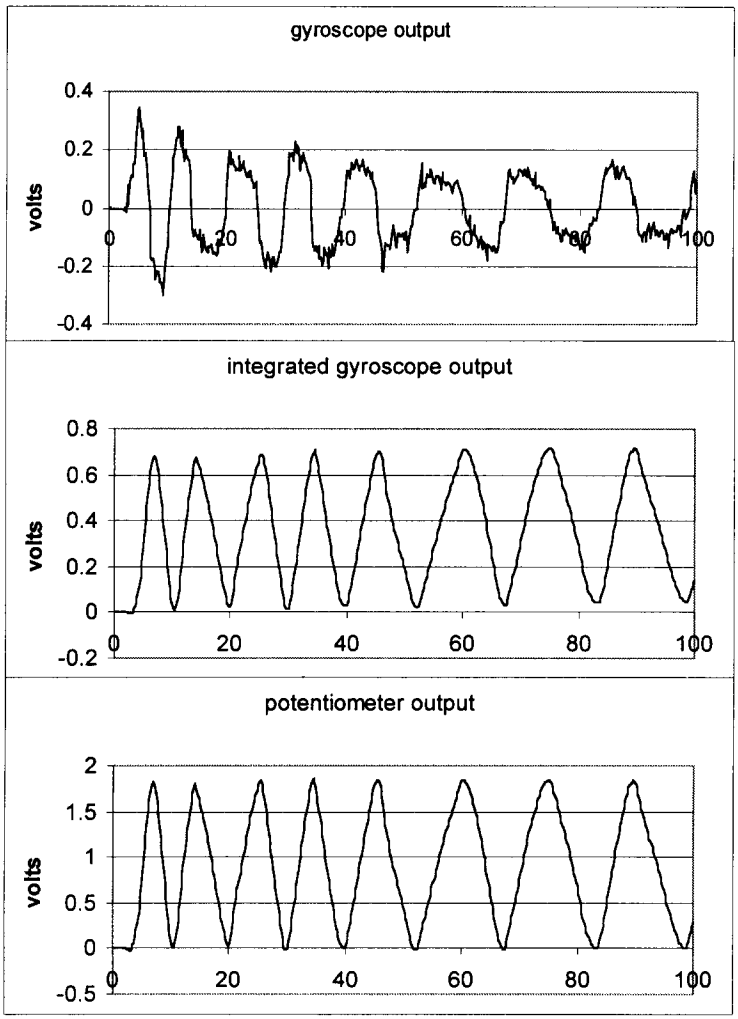

Figure 5: Time series plots of voltage output signals recorded from the gyroscope (top) and potentiometer (bottom). The middle plot present the integration of gyroscope output. The top trace is a measurement of the angular velocity of the signal, while the bottom traces are related to position. The angular excursion of the calibration device during this trial was approximately 90 degrees.

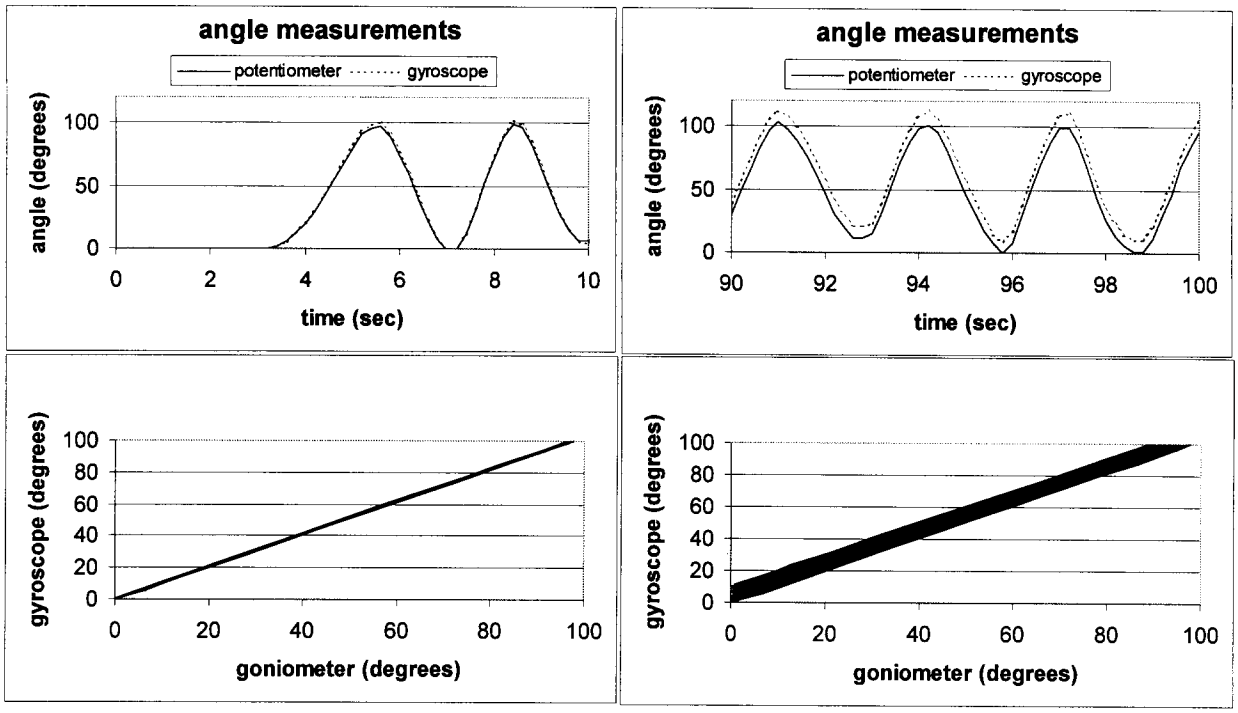

Figure 6: The top two plots show time series traces of the calibrated output from the potentiometer and the integrated output of the gyroscope. Data from these plots are taken from a trial that lasted 100 seconds: the first ten seconds of the trial is on the left; the last ten seconds are on the right. The bottom plots present the data in an x-y plot of goniometer vs. gyroscope: the plot on the left presents data from the first ten seconds of the trial; the plot on the right presents data from all 100 seconds of the trial. Note that initially, there is very good correspondence between the readings from the two sensors. However, there is significant drift in the integrated output from the gyroscope as seen in the two plots on the right.

References:

1. Andriacchi TP, Andersson GBJ, Fermier RW, Stern D, Galante JO, A Study of Lower Limb Mechanics During Stair Climbing, JBJS, Vol.62, pp.749-757, 1980.
2. Bressler B, Frankel F, The Forces and Moments in the Leg During Walking, Trans Am Soc Mech Engrs, Vol.72, pp.27-36, 1950.
3. Crowninshield RD, Johnston RC, Andrews JG, Brand RA, A Biomechanical Investigation of the Human Hip, J Biomechanics, Vol. 11, No.1, pp.75-85, 1978.
4. Riener R, Edrich T, Significance of Passive Elastic Joint Moments in FES, Proceedings of the Second Annual IFESS Conference (IFESS '97), pp.103-106.
5. Vrahas MS, Brand RA, Brown TD, Andrews JG, Contribution of Passive Tissues to the Intersegmental Moments at the Hip, J Biomechanics, Vol.23, No.4, pp.357-362, 1990.
6. Weiss PL, Kearney RE, Hunter IW, Position Dependence of Ankle Joint Dynamics –I. Passive Mechanics, J Biomechanics, Vol.19, No.9, pp.727-735, 1996.
7. Wright V, Johns RJ, Quantitative and Qualitative Analysis of Joint Stiffness in Normal Subjects and in Patients with Connective Tissue Diseases, Ann Rheum Dis, Vol.20, pp.36-46, 1961.